$^{40}Ar/^{39}Ar$ age, lithogeochemistry and petrographic studies of the Cretaceous Alkaline Marapicu Intrusion, Rio de Janeiro, Brazil

Idade $^{40}Ar/^{39}Ar$, litogeoquímica e estudos petrográficos da Intrusão Alcalina Cretácea do Marapicu, Rio de Janeiro, Brasil

Daniel Adelino da Silva[I], Mauro Cesar Geraldes[I], Thais Vargas[I],
Fred Jourdan[II], Camila Cardoso Nogueira[I]

[I]Universidade do Estado do Rio de Janeiro. Rio de Janeiro, Rio de Janeiro, Brasil

[II]Western Australian Argon Isotope Facility. Perth, Austrália

Abstract: The Marapicu Alkaline Massif is an intrusion into the Marapicu-Gericinó-Mendanha Igneous Complex that is part of the Cretaceous Poços de Caldas-Cabo Frio magmatic lineament located in the Southeastern region of Brazil. Nepheline syenites and phonolites are the most abundant rocks in the massif that also include syenites forming an alkaline series SiO_2-undersatured. Chemically this series is predominantly metaluminous and to a lesser extent peralkaline. This series presents both potassic and sodic suites being the first one in greater content. The data show that both basic and intermediary rocks with parental composition sampled in this area have no genetic relationship with the other rocks of the body. Geochemistry data shows that evolution processes involved fractional crystallization with or without continental crust assimilation and also indicates that this alkaline magma was generating from an enriched mantle source. The $^{40}Ar/^{39}Ar$ age of hornblende (extracted of nepheline syenite) from Marapicu massif is 80.46 ± 0.58 Ma, which it is contrasting, with the idea of age decrease of the hotspot track from west to east on the Poços de Caldas-Cabo Frio magmatic lineament.

Keywords: Alkaline rocks. Marapicu Alkaline Massif. Geochemistry. $^{40}Ar/^{39}Ar$ age.

Resumo: O Maciço Alcalino do Marapicu é uma intrusão do complexo ígneo Marapicu-Gericinó-Mendanha que faz parte do lineamento magmático Poços de Caldas-Cabo Frio, localizado na região sudeste do Brasil. Nefelina sienitos e fonolitos são as rochas mais abundantes nesse maciço, que também inclui sienitos, formando uma série insaturada em sílica. Quimicamente, esta série é predominantemente metaluminosa e, em menor grau, peralkalina. Ela possui uma suíte potássica (predominante) e outra sódica. Os dados mostram que as amostras de composição básica coletadas não possuem relação genética com as demais. Dados geoquímicos indicam um processo de evolução envolvendo cristalização fracionada com ou sem assimilação de crosta continental, além disso indicam que esse magma foi gerado em fonte mantélica enriquecida. A idade $^{40}Ar/^{39}Ar$ em hornblenda (extraída de nefelina sienito) do Marapicu é de 80,46 ± 0,58 Ma, contrastando com a ideia de decréscimo de idade do traço do *hot spot* de oeste para leste no lineamento Poços de Caldas-Cabo Frio.

Palavras-chave: Rochas alcalinas. Maciço alcalino do Marapicu. Geoquímica. Idade $^{40}Ar/^{39}Ar$.

SILVA, D. A., M. C. GERALDES, T. VARGAS, F. JOURDAN & C. C. NOGUEIRA, 2016. $^{40}Ar/^{39}Ar$ age, lithogeochemistry and petrographic studies of the Cretaceous Alkaline Marapicu Intrusion, Rio de Janeiro, Brazil. **Boletim do Museu Paraense Emílio Goeldi. Ciências Naturais** 10(3): 399-422.

Autor de correspondência: Daniel Adelino da Silva. Universidade do Estado do Rio de Janeiro. Programa de Pós-Graduação em Análise de Bacias e Faixas Móveis. Rua São Francisco Xavier, 524 – Maracanã. Rio de Janeiro, RJ, Brasil. CEP 20550-990 (adelinogeologia@yaoo.com.br).

Recebido em 28/04/2015
Aprovado em 07/04/2016
Responsabilidade editorial: Mário Augusto G. Jardim

INTRODUCTION

The Marapicu-Gericinó-Mendanha Igneous Complex (Figure 1) is composed of two adjacent alkaline intrusions named as Marapicu and Mendanha; these bodies are intruded into the Central segment of the Neoproterozoic Ribeira Mobile Belt and make part of the Brazilian Southeast Alkaline Province (Almeida, 1983). The Marapicu-Gericinó-Mendanha Igneous Complex is detached related to other alkaline provinces of the South America Platform for including plutonic, sub-volcanic (mainly dykes) and volcanic (rarely seen in that provinces) rocks (Ulbrich & Gomes, 1981). The Marapicu Massif forms a smaller body with approximately circular shape having close to 10 km^2 in area and height over 400 m. The Gericinó-Mendanha is the biggest body localized east side of the Marapicu and has approximately shape the ellipse. Its higher accessible point is over than 850 m. In this body is localized the Nova Iguaçu Volcanic Complex which is composed for central agglomerate, bombs, tuffs and abundant lapilli (Klein & Vieira, 1980; Klein, 1993). In this study, we carry out new petrographical observations and, geochemical and $^{40}Ar/^{39}Ar$ analyses of samples from the Marapicu Massif. The aim of this study is to constrain the emplacement models of the Cretaceous-Tertiary magmatism, which have taken place in the South-American Plate, southern from Brazil.

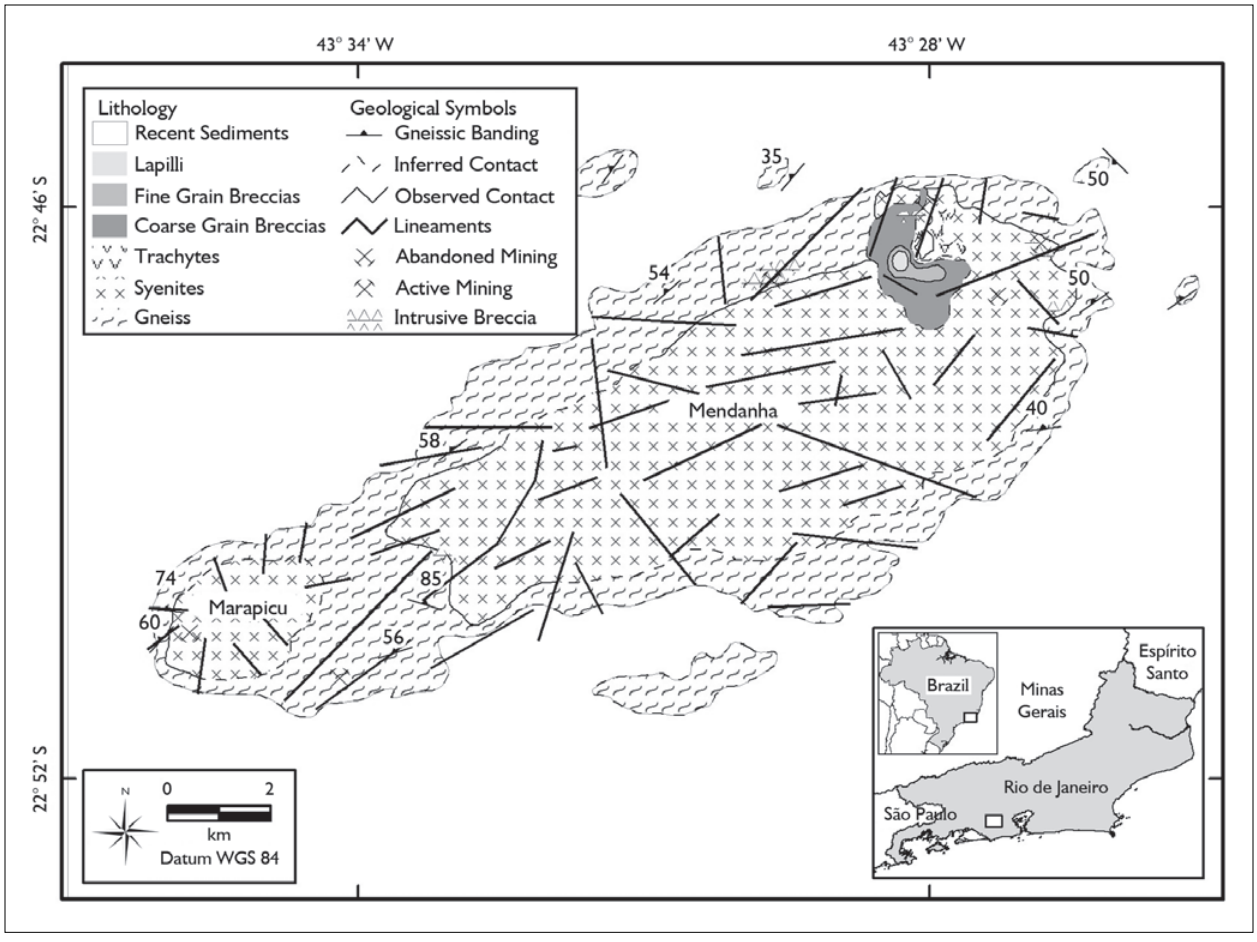

Figure 1. Geologic map of Marapicu massif (smaller body in the left) and Gericinó-Mendanha massif (bigger body in the right) adapted of Mota (2008).

TECTONIC SETTING

Alkaline rocks occurrence in the southeast part of Brazil are observed in two great magmatic lineaments of Cretaceous-Tertiary age in the South-American Platform. The first presents a NW-SE direction and is called Poços de Caldas-Cabo Frio Lineament (Figure 2) and the second which have a NW-SW direction is called Southern Coast (Ulbrich & Gomes, 1981). These two lineaments make part of the Alkaline Province of Brazilian Southern (Almeida, 1986).

The magmatism dated from Mesozoic to Cenozoic periods is widely registered on the Brazilian territory as tholeitic lava flows, dykes, alkaline plugs and stocks (Almeida, 1976, 1986; Almeida *et al*., 1996; Thomaz Filho & Rodrigues, 1999; Thomaz Filho *et al*., 2005).

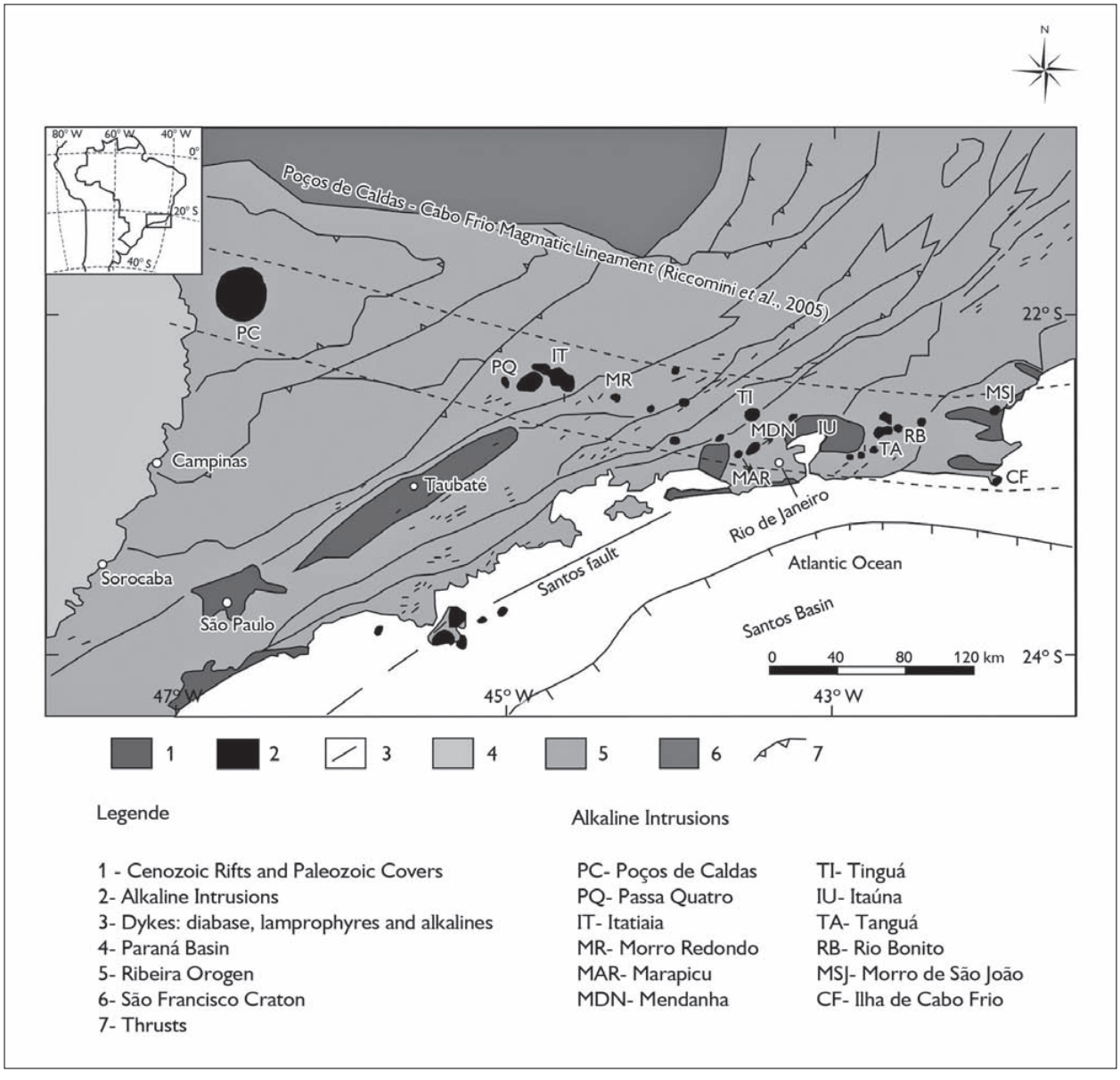

Figure 2. Poços de Caldas-Cabo Frio magmatic lineament.

These magmatic manifestations are associated with two great events, which occurred in the South-American Platform, stabilized in the Cambrian-Ordovician and, can be sub-divided in the tholeitic magmatism that is associated to Gondwana break-up and consequently opening of South Atlantic Ocean. These magmatic events occurred approximately 130 to 120 Myr ago and are associated with the implantation of a Brazilian passive margin basin. The other event is the alkaline magmatism related to uplift phenomena such as the occurred in the Serra do Mar and sedimentary tertiary basin of Brazilian southern formation.

The alkaline rock bodies' lineament Poços de Caldas-Cabo Frio (Almeida, 1983, 1986, 1991; Almeida *et al*., 1996; Freitas, 1947) form a located magmatic sequence represented by alkaline rocks in the form of stocks, plugs, dykes and rare lavas and pyroclastic flows. These rocks present ages between Upper Cretaceous to Eocene and setting in WNW-ESE direction into the Rio de Janeiro state, cutting by oblique way the preferential direction of tectonic structures from the Neoproterozoic Ribeira Mobile Belt. Almeida (1991) refers to that alkaline rocks being exclusively felsics and presented mainly for nepheline syenite, pulaskite, foiaite, phonolite, tinguaite and trachyte.

GEODYNAMIC MODELS

Three geodynamic models have been proposed for explaining the Upper Cretaceous alkaline magmatism in the meridional part of South-American Plate (Almeida, 1991; Fainstein & Summerhayes, 1982; Thomaz Filho *et al*., 2000; Thompson *et al*., 1998) as following: reactivation of deep faults; hotspot activity and; the combination of two previous models.

The reactivation of deep faults proposal is directly related to the sub-parallelism of both continental and oceanic lineaments observed in the Atlantic passive margin of the South-American Plate (for instance: Gorini & Bryan, 1976).

The plumes and hotspots related magmatism model (for instance: Gibson *et al*., 1995) suggest that the alkaline activity of Upper Cretaceous in the southern of Brasil may have been caused for the Trindade-Martin Vaz mantle plume at the base of continental lithosphere.

The third model attempted to associate the fault reactivation by the presence of a thermic anomaly (plume) in the Upper Cretaceous of the Brazilian southeast region (Fainstein & Summerhayes, 1982; Thomaz Filho *et al*., 2000). This model explains the magmatic activity related to the Poços de Caldas-Cabo Frio lineament as a response for the thermic anomaly also responsible for the formation of the Vitoria-Trindade magmatic lineament.

MATERIALS AND METHODS

FIELD WORK

The methodology applied in this study starting with fieldwork when 28 outcrops were visited at the parts Southwest, North and Northeast of the area and 52 samples were collected. The greater part of the sampling includes nepheline syenites and phonolites, which are the most representatives in the area. Furthermore, we have collected one basanite/tefrite and one tefrite phonolitic. The nepheline syenites and syenites presents granulometry ranging from fine to coarse including pegmatitic types. The plutonic rocks occur intruded into the granites and gneiss of the Domínio Costeiro from the Ribeira Mobile Belt, the phonolites occur as hipoabissal bodies the way of the dikes with up to 3 m width. These dikes have two main trends: NW-SE e NNE-SSW.

$^{40}Ar/^{39}Ar$ METHODOLOGY

We selected a fresh sample from Marapicu for $^{40}Ar/^{39}Ar$ dating and separated unaltered, optically transparent, 250-500 μm size, hornblende. These minerals were separated using a Frantz magnetic separator, and then carefully hand-picked under a binocular microscope. The selected hornblende minerals were further leached in diluted HF for one minute and then thoroughly rinsed with distilled water in an ultrasonic cleaner. This step was carried out at the Geologic Laboratory of Sample Preparation from State University of Rio de Janeiro.

After the hornblende grain separation the $^{40}Ar/^{39}Ar$ dating was carried out at the Curtin University from Australia where the Samples were loaded into a large wells of 1.9 cm diameter and 0.3 cm depth aluminum disc. This well was bracketed by small wells that included Fish Canyon sanidine (FCs) used as a neutron fluence monitor for which an age of 28.294 ± 0.036 Ma (1σ) was adopted of Renne *et al*. (2011). The discs were Cd-shielded (to minimize undesirable nuclear interference reactions) and irradiated for 2 hours in the Hamilton McMaster University nuclear reactor (Canada) in position 5C. The mean J-values computed from standard grains within the small pits and determined as the average and standard deviation of J-values of the small wells for each irradiation disc is given along with the raw data in Table 1. Mass discrimination is given in Table 2 for each sample and was monitored using an automated air pipette and calculated relative to an air ratio of 298.56 ± 0.31 (Lee *et al*., 2006). The correction factors for interfering isotopes were $(^{39}Ar/^{37}Ar)_{Ca}$ = 7.30x10-4 (± 11%), $(^{36}Ar/^{37}Ar)_{Ca}$ = 2.82x10-4 (± 1%) and $(^{40}Ar/^{39}Ar)_{K}$ = 6.76x10-4 (± 32).

The $^{40}Ar/^{39}Ar$ analyses were performed at the Western Australian Argon Isotope Facility at Curtin University. The sample was step-heated in a double vacuum high frequency Pond Engineering© furnace. The gas was purified in a stainless steel extraction line using two AP10 and one GP50 SAES getters and a liquid nitrogen condensation trap. Ar isotopes were measured in static mode using a MAP 215-50 mass spectrometer (resolution of ~400; sensitivity of 4 x 10^{-14} mol/V) with a Balzers SEV 217 electron multiplier using 9 to 10 cycles of peak-hopping.

The data acquisition was performed with the Argus program written by M.O. McWilliams and ran under a LabView environment. The raw data were processed using the ArArCALC software (Koppers, 2002) and the ages have been calculated using the decay constants recommended by Renne *et al*. (2011). Blanks were monitored every 3 to 4 steps and typical ^{40}Ar blanks range from 1 x 10^{-16} to 2 x 10^{-16} mol. Ar isotopic data corrected for blank, mass discrimination and radioactive decay are given in Table 3. Individual errors in Table 3 are given at the 1σ level.

Table 1. Mean J-values.

Sample	Material	Location	Temp	Standard age (in Ma)	%1σ	J	%1σ	MDF	%1σ	Volume ratio	Sensibility (mol/vol)	Irradiation	Standard name
MPC-11	Hbl	Furnace	600 °C	28,305	0,13	0,009182	0,29	1,000554	0,32	1	4,020E-14	I7t25h	FCs
MPC-11	Hbl	Furnace	700 °C	28,305	0,13	0,009182	0,29	1,000554	0,32	1	4,020E-14	I7t25h	FCs
MPC-11	Hbl	Furnace	800 °C	28,305	0,13	0,009182	0,29	1,000554	0,32	1	4,020E-14	I7t25h	FCs
MPC-11	Hbl	Furnace	900 °C	28,305	0,13	0,009182	0,29	1,000554	0,32	1	4,020E-14	I7t25h	FCs
MPC-11	Hbl	Furnace	1000 °C	28,305	0,13	0,009182	0,29	1,000554	0,32	1	4,020E-14	I7t25h	FCs
MPC-11	Hbl	Furnace	1025 °C	28,305	0,13	0,009182	0,29	1,000554	0,32	1	4,020E-14	I7t25h	FCs
MPC-11	Hbl	Furnace	1050 °C	28,305	0,13	0,009182	0,29	1,000554	0,32	1	4,020E-14	I7t25h	FCs
MPC-11	Hbl	Furnace	1075 °C	28,305	0,13	0,009182	0,29	1,000554	0,32	1	4,020E-14	I7t25h	FCs
MPC-11	Hbl	Furnace	1100 °C	28,305	0,13	0,009182	0,29	1,000554	0,32	1	4,020E-14	I7t25h	FCs
MPC-11	Hbl	Furnace	1125 °C	28,305	0,13	0,009182	0,29	1,000554	0,32	1	4,020E-14	I7t25h	FCs
MPC-11	Hbl	Furnace	1150 °C	28,305	0,13	0,009182	0,29	1,000554	0,32	1	4,020E-14	I7t25h	FCs
MPC-11	Hbl	Furnace	1175 °C	28,305	0,13	0,009182	0,29	1,000554	0,32	1	4,020E-14	I7t25h	FCs

Table 2. Mass discrimination for each step.

Temp	36Ar(a)	36Ar(c)	36Ar(ca)	36Ar(cl)	37Ar(ca)	38Ar(a)	38Ar(c)	38Ar(k)	38Ar(ca)	38Ar(cl)	39Ar(k)	39Ar(ca)	40Ar(r)	40Ar(a)	40Ar(c)	40Ar(k)
600 °C	0,000056	0,000000	0,000003	0,000000	0,009019	0,000011	0,000000	0,000341	0,000000	0,000039	0,027463	0,000007	0,135544	0,016653	0,000000	0,000019
700 °C	0,000332	0,000000	0,000006	0,000000	0,021482	0,000062	0,000000	0,000649	0,000000	0,000188	0,052323	0,000016	0,267687	0,097959	0,000000	0,000035
800 °C	0,000171	0,000000	0,000014	0,000000	0,049748	0,000032	0,000000	0,001118	0,000001	0,000280	0,090133	0,000036	0,451279	0,050443	0,000000	0,000061
900 °C	0,000290	0,000000	0,000347	0,000001	1,229999	0,000054	0,000000	0,007489	0,000028	0,000280	0,603973	0,000898	2,969755	0,085840	0,000000	0,000408
1000 °C	0,000447	0,000000	0,001595	0,000006	5,654463	0,000084	0,000000	0,025820	0,000129	0,021060	2,082239	0,004128	10,22180	0,132229	0,000000	0,001408
1025 °C	0,000040	0,000000	0,000060	0,000000	0,214505	0,000007	0,000000	0,009942	0,000005	0,000689	0,075966	0,000157	0,370165	0,011820	0,000000	0,000051
1050 °C	0,000050	0,000000	0,000078	0,000000	0,275759	0,000009	0,000000	0,001162	0,000006	0,000994	0,093739	0,000201	0,457060	0,014839	0,000000	0,000063
1075 °C	0,000152	0,000000	0,000523	0,000002	1,854233	0,000028	0,000000	0,007466	0,000042	0,005902	0,602129	0,001354	2,965516	0,044810	0,000000	0,000407
1100 °C	0,000052	0,000000	0,000448	0,000001	1,588297	0,000010	0,000000	0,005169	0,000036	0,003773	0,416832	0,001159	2,055986	0,015355	0,000000	0,000282
1125 °C	0,000027	0,000000	0,000068	0,000000	0,242502	0,000005	0,000000	0,000648	0,000006	0,000571	0,052251	0,000177	0,256844	0,007869	0,000000	0,000035
1150 °C	0,000046	0,000000	0,000012	0,000000	0,043352	0,000009	0,000000	0,000146	0,000001	0,000076	0,011748	0,000032	0,049608	0,013702	0,000000	0,000008
1175 °C	0,000061	0,000000	0,000012	0,000000	0,041620	0,000011	0,000000	0,000142	0,000001	0,000130	0,011476	0,000030	0,048346	0,017919	0,000000	0,000008

Table 3. Ar isotopic data corrected for blank, mass discrimination and radioactive decay.

Temp.	40(r)/ 39(k)	1σ	40(r+a)	1σ	40Ar/ 39Ar	1σ	37Ar/ 39Ar	1σ	36Ar/ 39Ar	1σ	37Ar (decay)	39Ar (decay)	40Ar (moles)
600 °C	4,935491	0,18010	0,15220	0,00132	5,54120	0,05637	0,32832	0,04230	0,00214	0,00058	27,99711685	1,00119105	6,119E-15
700 °C	5,116062	0,11540	0,36565	0,00133	6,98685	0,03861	0,41045	0,02129	0,00645	0,00037	28,01709338	1,00119130	1,470E-14
800 °C	5,006840	0,05874	0,50172	0,00142	5,56493	0,02630	0,55172	0,02390	0,00205	0,00018	28,03708417	1,00119156	2,017E-14
900 °C	4,917031	0,02349	3,05559	0,00242	5,05232	0,01733	2,03349	0,07059	0,00106	0,00005	28,05670437	1,00119181	1,229E-13
1000 °C	4,909047	0,01985	10,35404	0,00881	4,96339	0,01732	2,71020	0,09362	0,00098	0,00002	28,07441280	1,00119203	4,163E-13
1025 °C	4,872760	0,08593	0,38198	0,00134	5,01869	0,02892	2,81788	0,10224	0,00132	0,00027	28,09444449	1,00119229	1,536E-14
1050 °C	4,875871	0,05313	0,47190	0,00130	5,02406	0,02434	2,93547	0,10679	0,00137	0,00016	28,11410483	1,00119254	1,897E-14
1075 °C	4,925050	0,02119	3,01033	0,00202	4,98893	0,01659	3,07255	0,10638	0,00112	0,00003	28,13377894	1,00119279	1,210E-13
1100 °C	4,932413	0,02733	2,07134	0,00176	4,95614	0,01793	3,79984	0,13165	0,00120	0,00006	28,15346681	1,00119304	8,328E-14
1125 °C	4,915601	0,11410	0,26471	0,00132	5,04978	0,03411	4,62545	0,16329	0,00182	0,00036	28,17316846	1,00119329	1,064E-14
1150 °C	4,222606	0,50306	0,06331	0,00125	5,37514	0,11364	3,68020	0,16580	0,00498	0,00166	28,19211048	1,00119353	2,545E-15
1175 °C	4,212596	0,38884	0,06626	0,00105	5,75936	0,10206	3,61702	0,16169	0,00629	0,00127	28,21183917	1,00119378	2,664E-15

Our criteria for the determination of plateau are as follows: plateaus must include at least 70% of ^{39}Ar. The plateau should be distributed over a minimum of 3 consecutive steps agreeing at 95% confidence level and satisfying a probability of fit (P) of at least 0.05. Plateau ages are given at the 2σ level and are calculated using the mean of the entire plateau steps, each weighted by the inverse variance of their individual analytical error. Inverse isochrons include the maximum number of steps with a probability of fit $\geq$ 0.05. The $^{40}Ar/^{36}Ar$ intercept value is provided. All sources of uncertainties are included in the calculation.

PETROGRAPHY

Nepheline syenite and syenite

The plutonic lithotypes include nepheline syenites and syenites showing very similar petrographic and hand sample characteristics, they presents holocrystalline and equigranular texture and grain size ranging from coarse (3 to 6 mm) to fine (± 1 m) (Figures 3A, 3B and 3C). Its main mineralogy include: alkali feldspar, nepheline, plagioclase and hornblende. The accessory minerals include: biotite, scapolite, muscovite, carbonate, zircon, apatite, augite and opaque mineral (mainly magnetite). Fine-grained white clay mineral is common in all samples, formed by the decomposition of alkali feldspar.

The alkali feldspar grains with simple Carlsbad twins and plagioclase both occur in different shapes anhedral, subhedral and tabular euhedral, they have coarse (3 to 6 mm) to medium sizes (1 to 3 mm). Abundant alkali feldspar grains are microperthitic (Figures 3D and 3F) and show transformation into very fine ragged grains of sericite and ultrafine – grained clay with a cloudy appearance, a radial texture is present too (Figure 3D). The plagioclase with K-feldspar lamellae also shows an alteration grade, which occults almost totally its polysynthetic twinning. The nepheline occurs, in smaller proportion related to feldspars, with anhedric and subhedric coarse crystals and takes place in interstitial spaces.

The hornblende grains are strongly pleochroic from greenish-brown to dark brown, occur in anhedral, subhedral and euhedral shapes forming hexagonal grains. Some zoned

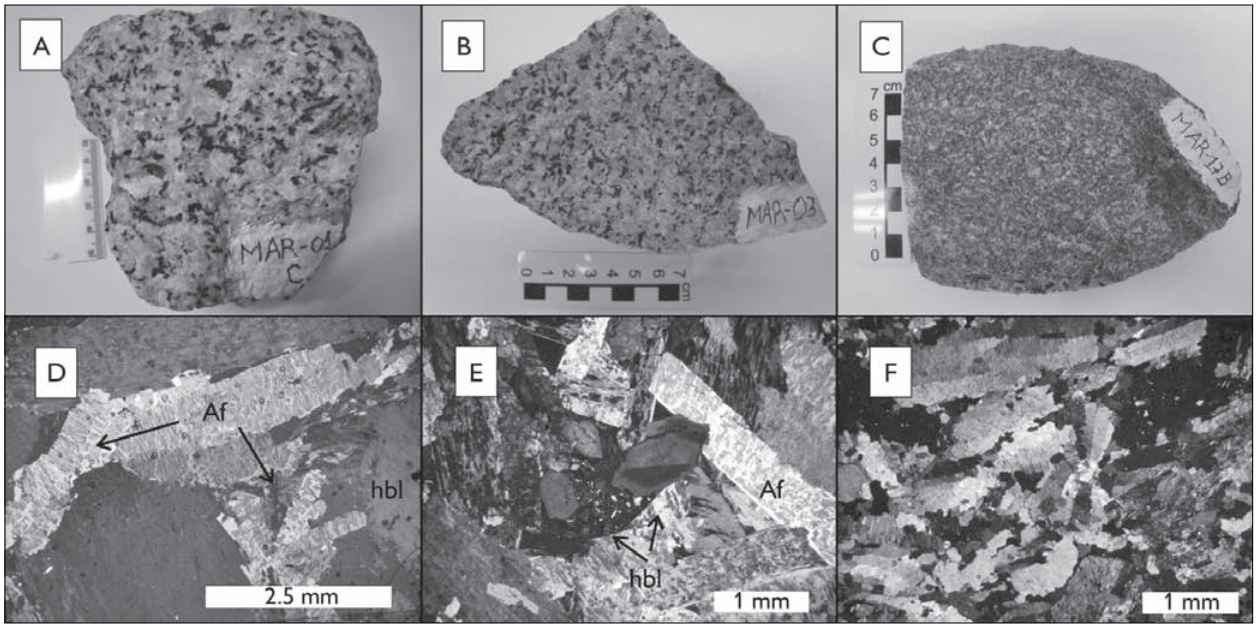

Figure 3. Characteristics of the facies syenitic: A, B and C) macroscopic aspect of the handle sample; D, E and F) photomicrographs in cross-polarized light. Legends: Af = alkali feldspar; hbl = hornblende.

grains present a variation of green colour being more dark in the rim and more light in the core, besides the simple twinning visible (Figure 3E). Other aspect is that the hornblende presents inclusions of apatite and biotite (more often), but opaque minerals, scapolite and carbonate are also observed. In their rim occur grains of biotite and opaque minerals, muscovite sometimes as alteration product is present too.

The biotite is observed forming anhedral and subhedral grains or as rips. It appears as inclusion in hornblende or in contact with their rims. The apatite is sub-milimetric, also disseminated and occurs commonly included in hornblende, as anhedral and euhedral grains with hexagonal or neddle habits. The scapolite occurs frequently as xenomorphic crystals but few present triangular habits. Carbonate, muscovite, augite and opaque mineral are found in subordinated amount. Opaque minerals are mainly magnetite forming few grains with anhedral habit. Zircon is rare and generally occurs < 1 mm in size.

Phonolites

The phonolites can be divided in two groups based on their phenocrysts content. The first group of phonolite is represented by a fine-grained, inequigranular porphyritic rock (Figure 4A) with phenocrysts of alkali-feldspar, nepheline and hornblende that comprise ~10% by volume of the rock (Figure 4C) in a hypocrystalline matrix.

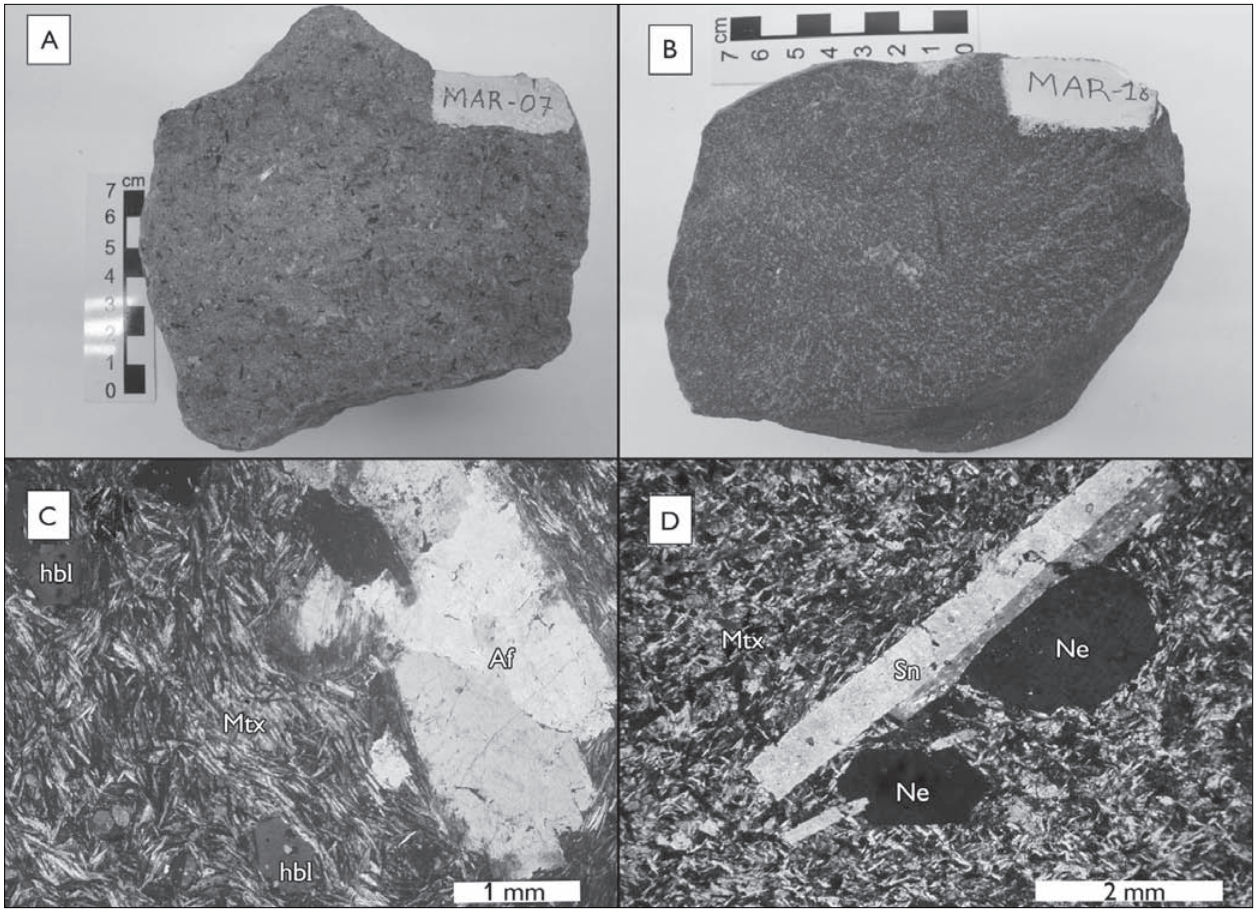

Figure 4. Characteristics of the two phonolite groups, (A) macroscopic aspect of the phonolite of first group, (B) macroscopic aspect of phonolite of second type, (C) photomicrograph them with a strong trachytic texture in cross-polarized light, and (D) photomicrograph them, in cross-polarized light. Legends: Ne = nepheline; Sn = sanidine; Af = alkali feldspar; hbl = hornblende; Mtx = matrix.

The groundmass of the rock has a grain size < 1 mm. It exhibits a strong trachytic texture, and is dominated by sanidine, hornblende and biotite. The alkali feldspar phenocrysts show Carlsbad twinning and large size (3 to 5 mm), are anhedral and subhedral with tabular habit. The nepheline phenocrysts are subhedral and euhedral with hexagonal habit occurring as medium sized crystals (2 to 3 mm). Hornblende phenocrysts are anhedral and euhedral and up 3 mm with hexagonal, octagonal and tabular habits. Some grains present compositional zoning and carlsbad twinning. Isotropic glass and opaques occur within interstitial areas.

The second type of phonolite (Figure 4B) is a rock inequigranular porphyritic with a fine-grained matrix and phenocrystals of sanidine and nepheline, which have a medium size (about 3 mm), also occur a few millimetric phenocrysts of biotite. The accessory minerals are biotite, scapolite, augite, opaque minerals and zircon. The sanidine integrates the matrix forming submilimetric crystals commonly subhedral and euhedral. It is common their presence as euhedral phenocrysts with tabular habit and carlsbad twinning. Many sanidine grains are elongate laths (Figure 3D). The nepheline occurs as subhedral and euhedral phenocrystals, with hexagonal habit. Microscopic examination reveals the trachytic texture of the fine matrix.

Whole rock Geochemistry

A subset of 27 samples was prepared for whole rock geochemical analyses at the Geologic Laboratory of Sample Preparation from State University of Rio de Janeiro. The hand sample were cut the way of chip being two pieces for each sample and them these chips were fragmented in a pestle. The fragments were washed with distilled water and alcohol so left to dry. These fragments were powdered in a tungsten ball mill; this machine is also a mixer ensuring the homogeneity of the sample. The rock powder for each sample is stored in 10 g container and then send to geochemical analyses.

All geochemical analyses were performed in the Activation Laboratories Ltd. from Canada by using relatively fresh samples. Whole rock major and trace element concentrations were measured using Fusion Mass Spectrometry (FUS-MS) and Fusion Inductively Coupled Plasma (FUS-ICP) techniques. The sum of the major elements and Loss on Ignition is between 98.19 and 100.55 wt%. The Loss on Ignition values are less than 5%. The iron analyses were carried out in the way of total Fe_2O_3 as indicated in Appendix.

The Marapicu massif is constituted of an alkaline series, which have mainly nepheline syenites and phonolites as it is shown in the Figure 5. This series it is characterized for increasing of the alkalis (Na_2O+K_2O) content along with decreasing of the SiO_2 content, in this way, geochemically the more evaluated members of the series are the phonolites and the less evaluated members are the syenites.

The samples analyzed form an alkaline series with intermediary character and SiO_2 content ranging of 53.46 wt% to 61.87 wt%. Into the TAS diagram (SiO_2 *versus* Na_2O+K_2O) of Cox *et al*. (1979), the most part of the samples lie in the nepheline syenite field, and a smaller group lie in the syenite field. The sample MAR-28C have a basic composition with SiO_2 content of 47.5 wt% and high content of Fe_2O_3T (8.24 wt%), MgO (7.02 wt%) and CaO (8.51 wt%) which are mafic rock-forming mineral elements, besides, presents both high content of Ni (130 ppm) and Cr (370 ppm). This way the sample cited would be representative the parental magma of the alkaline serie in study but as will be showed there is no genetic relationship with the other samples. The sample MAR-24 also have a mafic composition with high content of Fe_2O_3T (9.01 wt%), MgO (2.5 wt%) and CaO (5.66) and have not genetic relationship with the other samples too.

The A/CNK *versus* A/NK (Al/2Ca+Na+K *versus* Al/Na+K molar prop.) by Shand (1943) (Figure 6) was used to discriminate the alumina saturation classes. According to this diagram the most part of the samples (all of the plutonic nepheline syenites and syenites in addition to part of the phonolites) are metaluminous (Al_2O_3/Na_2O+K_2O > 1), which indicate that had excess of Ca

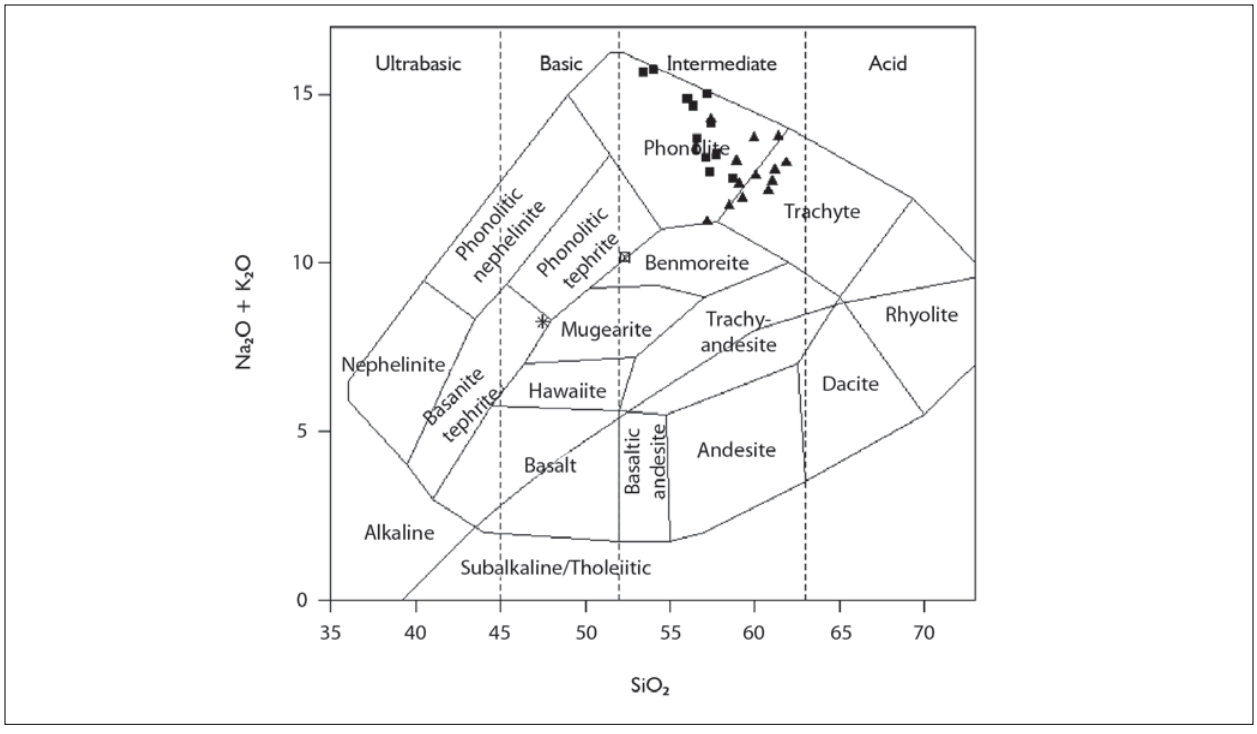

Figure 5. Total alkalis *versus* silica chemistry classification diagram by Cox *et al*. (1979) for all Marapicu samples analized. Triangle represents plutonic nepheline syenites and syenites, filled squares represents phonolites, open square and asterisk represents basic rocks.

after the alumina cumulate on feldspar, this is agreed with mineral assemblage formed for hornblende and biotite observed in the petrography. A lesser part of the samples (phonolites not included in the metaluminous group) are peralkalines ($Al_2O_3/Na_2O+K_2O < 1$), and indicating an excess of alkalis related to alumina and more alkalis that the necessary to make feldspars, as agreed with hornblende present in the mode. Furthermore the sample MAR-19A (nepheline syenite) presents peraluminous character (Al/(2Ca+Na+K)) indicating more alumina than necessary to make feldspar and corroborated by normative corundum (Table 4). The CIPW norm applied these samples show that it is a SiO_2-undersatured series including a normative assemblage of *Or+Ab±An+Ne±Di±Ol* (Table 4). This way, metaluminous plutonic nepheline syenites and syenites are anorthite and diopside normatives. On the other hand, peralkaline volcanic phonolite presents sodium metasilicate (Ns) and lack of anorthite in the norm.

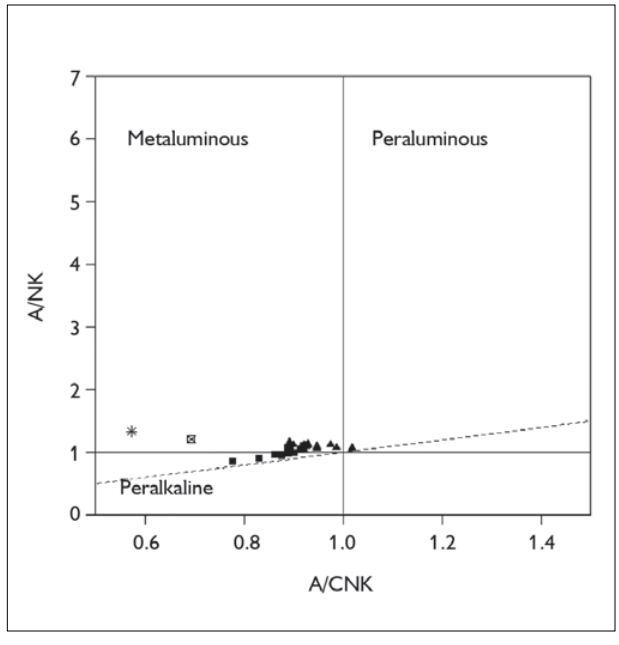

Figure 6. Aluminosity diagram by Shand (1943) showing predominant metaluminous samples. Triangle represents plutonic nepheline syenites and syenites, filled squares represents phonolites.

Table 4. CIPW (Cross, Iddings, Pirrson and Washington - the creators of the norm calculation) norm of the 27 analyzed samples from Marapicu massif. The normative minerals keys are: Q = quartz, C = corundum, Or = orthoclase, Ab = albite, An = anortite, Ne = nepheline, Ns = nosean, Di = diopside, Wo = wolastonite, Hy = hyperstene, Ol = olivine, Il = ilmenite, Tn = titanite, Pf = plagioclase, Ru = rutile, Ap = apatite. (Continue)

Analyte symbol	Classification	Q	C	Or	Ab	An	Ne	Ns	Di	Wo	Hy	Ol	Il	Tn	Pf	Ru	Ap	Sum
MAR-28C	Basanite/ tephrite	0.000	0.000	20.034	16.421	10.557	13.428	0.000	18.658	0.000	0.000	6.192	0.336	0.000	2.323	0.000	1.066	89.015
MAR-24	Phonolitic tephrite	0.000	0.000	29.726	30.538	7.857	7.018	0.000	9.326	0.000	0.000	1.334	0.586	0.000	2.017	0.000	1.492	89.894
MAR-06A	Phonolite	0.000	0.000	36.226	39.133	4.792	8.917	0.000	1.881	0.200	0.000	0.000	0.319	0.000	0.426	0.000	0.261	92.155
MAR-07	Phonolite	0.000	0.000	37.172	37.442	4.495	11.438	0.000	1.934	0.167	0.000	0.000	0.332	0.000	0.464	0.000	0.308	93.751
MAR-22B	Phonolite	0.000	0.000	34.808	44.296	3.295	6.395	0.000	2.418	0.499	0.000	0.000	0.509	0.000	0.353	0.000	0.474	93.047
MAR-19B	Phonolite	0.000	0.000	35.104	40.018	2.342	11.234	0.000	0.913	1.232	0.000	0.000	0.362	0.000	0.115	0.000	0.142	91.462
MAR-05A	Phonolite	0.000	0.000	35.340	37.456	1.683	13.676	0.000	1.113	1.257	0.000	0.000	0.325	0.000	0.000	0.000	0.166	91.016
MAR-04C	Phonolite	0.000	0.000	36.167	36.654	0.532	14.752	0.000	1.134	1.787	0.000	0.000	0.334	0.000	0.000	0.000	0.166	91.526
MAR-18	Phonolite	0.000	0.000	34.217	33.241	0.000	22.710	0.389	0.573	1.872	0.000	0.000	0.139	0.000	0.000	0.000	0.024	93.164
MAR-22C	Phonolite	0.000	0.000	33.390	36.109	0.000	19.962	0.744	0.806	1.368	0.000	0.000	0.287	0.000	0.191	0.000	0.166	93.022
MAR-28B	Phonolite	0.000	0.000	31.144	41.579	0.000	15.916	0.973	1.451	1.300	0.000	0.000	0.406	0.000	0.286	0.000	0.213	93.269
MAR-09A	Phonolite	0.000	0.000	33.981	36.490	0.000	19.593	1.306	0.797	1.504	0.000	0.000	0.281	0.000	0.000	0.000	0.095	94.047
MAR-02B	Phonolite	0.000	0.000	35.990	27.029	0.000	22.969	2.866	0.487	1.567	0.000	0.000	0.464	0.000	0.000	0.000	0.071	91.442

Table 4. (Conclusion)

Analyte symbol	Classification	Q	C	Or	Ab	An	Ne	Ns	Di	Wo	Hy	Ol	Il	Tn	Pf	Ru	Ap	Sum
MAR-15	Phonolite	0.000	0.000	29.253	31.844	0.000	21.820	4.306	0.662	1.789	0.000	0.000	0.467	0.000	0.000	0.000	0.095	90.237
MAR-27	Nepheline syenite	0.000	0.000	31.794	45.921	6.482	1.848	0.000	1.846	0.000	0.000	0.954	0.477	0.000	0.625	0.000	0.805	90.752
MAR-03	Nepheline syenite	0.000	0.000	37.467	43.566	4.848	3.903	0.000	1.460	0.587	0.000	0.000	0.435	0.000	0.000	0.000	0.237	92.503
MAR-10B	Nepheline syenite	0.000	0.000	32.740	38.082	3.760	19.342	0.000	0.444	0.000	0.000	0.025	0.154	0.000	0.000	0.000	0.095	94.642
MAR-19A	Nepheline syenite	0.000	0.489	32.858	51.151	1.707	9.787	0.000	0.000	0.000	0.000	0.111	0.048	0.000	0.000	0.000	0.118	96.269
MAR-01D	Nepheline syenite	0.000	0.000	35.931	43.341	2.874	11.451	0.000	0.605	0.930	0.000	0.000	0.139	0.000	0.000	0.000	0.047	95.317
MAR-17B	Nepheline syenite	0.000	0.000	33.272	46.020	2.124	8.945	0.000	0.693	1.336	0.000	0.000	0.276	0.000	0.000	0.000	0.118	92.784
MAR-20	Syenite	0.000	0.000	35.104	47.280	5.328	1.799	0.000	1.451	0.306	0.000	0.000	0.366	0.000	0.149	0.000	0.308	92.090
MAR-26	Syenite	0.000	0.000	31.912	47.897	5.231	2.886	0.000	2.279	0.000	0.000	0.359	0.317	0.000	0.508	0.000	0.568	91.958
MAR-06B	Syenite	0.000	0.000	37.881	47.627	5.271	3.262	0.000	0.302	0.000	0.000	0.199	0.205	0.000	0.172	0.000	0.213	95.131
MAR-16C	Syenite	0.000	0.000	36.876	48.386	4.973	0.742	0.000	1.934	0.237	0.000	0.000	0.332	0.000	0.244	0.000	0.237	93.960
MAR-01A	Syenite	0.000	0.000	37.113	48.721	4.087	1.706	0.000	1.236	0.621	0.000	0.000	0.274	0.000	0.189	0.000	0.213	94.159
MAR-16A	Syenite	0.000	0.000	37.940	47.998	4.271	4.023	0.000	1.075	0.314	0.000	0.000	0.233	0.000	0.155	0.000	0.189	96.199
MAR-13C	Syenite	0.000	0.000	36.758	45.927	4.060	4.320	0.000	1.558	0.461	0.000	0.000	0.302	0.000	0.244	0.000	0.261	93.891

Harker diagrams were confectioned for major elements K_2O, Na_2O, CaO, TiO_2, P_2O_5, $Fe_2O_3(T)$, MgO, Al_2O_3 (Figure 7) and also for the following trace elements Y, Rb, U, Eu, Pb, Ba, Sr and Th (Figure 8). The Figure 7 shows that Al_2O_3 ($R^2 = 0.0744$), and TiO_2 ($R^2 = 0.0811$) content roughly decrease with SiO_2 increase, Fe_2O_3 presents the same behavior although with better linear correlation ($R^2 = 0.1818$). MgO ($R^2 = 0.0089$), CaO ($R^2 = 0.0323$) and P_2O_5 ($R^2 = 0.0159$) roughly increase along with SiO_2. In fact, the R^2 values (linear correlation) for these oxides indicate dispersion of the data. Still looking in Figure 7, Na_2O content decrease with SiO_2 increase ($R^2 = 0.4653$), whereas K_2O ($R^2 = 0.2509$) content increase along with SiO_2. This way, only both Na_2O and K_2O presents robust linear correlation. The Figure 8 shows that Rb ($R^2 = 0.5697$), U ($R^2 = 0.1604$), Th ($R^2 = 0.4104$), Y ($R^2 = 0.6370$) and Pb ($R^2 = 0.5426$) content decrease with SiO_2 increase. All of these trace elements present robust data according to their R^2 values. On the other hand, Ba ($R^2 = 0.1842$), Sr ($R^2 = 0.1368$) and Eu ($R^2 = 0.0542$) content increase along with SiO_2 with poor linear correlation except for Ba.

Rare earth elements (REE) of the alkaline series were normalized to chondrite Boynton (1984) (Figure 9). This diagram showed that the REE pattern for the most part of the samples have in general a Eu negative anomaly, moreover, there is a bigger fractionating for the light REE (La, Ce, Pr, Nd, Pm, Sm) being more than one hundred times the condritic values related to heavy REE (Gd, Tb, Dy, Ho, Er, Tm, Yb, Lu). The samples MAR-28C and MAR-24 (basanite tephrite and phonolitic tephrite respectively) presents unexpectedly high REE content indicating lack of cogeneticity with the alkaline series studied. The high concentration of light REE suggests a source rich in these elements and the Eu negative anomaly suggest the fractionation of plagioclase in the least stages of the crystallization in addition to the fractionating of K-feldspar. The primitive mantle normalized spidergram by Sun & McDonough (1989) of the Figure 10 shows that the comportment of the elements of the Marapicu magma relate to their possibly mantle source. This diagram show a general pattern to which occurs a progressive depletion of Ba, Sr, P, and Ti, on the other hand, the remaining of the more incompatible REE elements are enriched.

RESULTS AND DISCUSSION

The $^{40}Ar/^{39}Ar$ dating of the Marapicu intrusion has been carried out by using hornblende grain extracted of the nepheline syenite sample as above mentioned. The hornblende sample yielded a plateau age of 80.46 ± 0.58 Ma (MSWD = 1.08; P = 0.37) including 100% of the ^{39}Ar released (Figure 11) that we interpret as the cooling age of the hornblende, which should be temporally very close to indistinguishable from its crystallization age.

The K/Ca ratio (derived from the $^{39}Ar/^{37}Ar$ ratio) shows the presence of a K-rich component at the low-temperature steps (Figure 12), but show a relatively constant composition (~0.2) for the medium to high temperature steps, suggesting that the selected crystals were homogenous and did not contain any inclusions.

The data were plotted in an inverse isochron diagram (Figure 13) and gave an age of 80.27 ± 0.62 Ma statistically indistinguishable from the plateau age, and a $^{40}Ar/^{36}Ar$ ratio of 326 ± 36, indistinguishable from atmospheric composition. This suggest that no excess $^{40}Ar^*$ is present in the sample.

The present data suggest that the Marapicu massif form an alkaline series mostly constituted of phonolites and nepheline syenites. This series has SiO_2-undersatured character and it is observed SiO_2 decreasing along with alkalis (Na_2O+K_2O) increasing in the TAS diagram. Binary diagrams from Marapicu massif samples present linear correlations without large compositional variations, which it is indicative of fractional crystallization with or without assimilation.

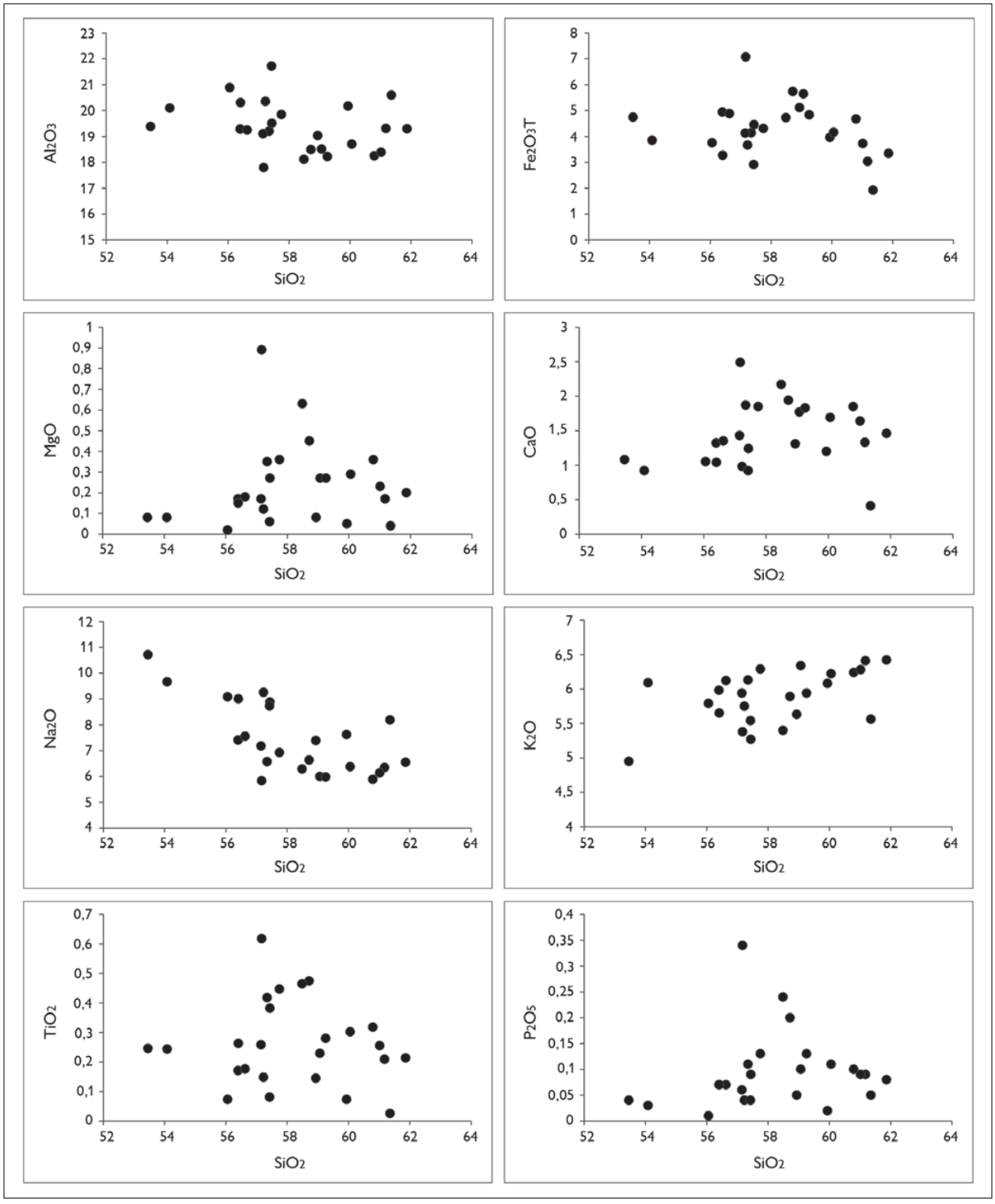

Figure 7. Harker diagrams for major elements from Marapicu Alkaline Massif. Samples MAR-24 and MAR-28C were not ploted.

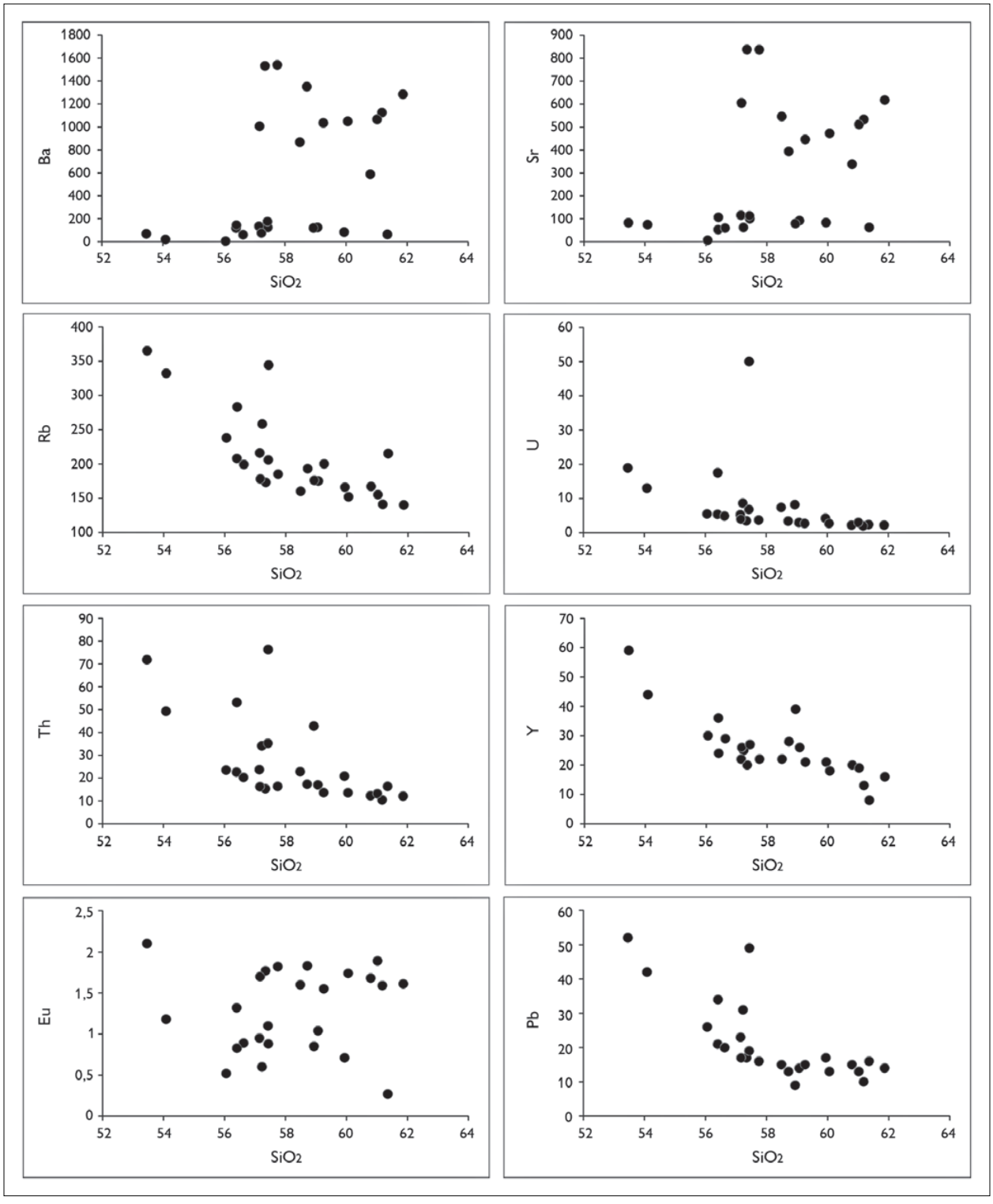

Figure 8. Harker diagrams for trace elements from Marapicu Alkaline massif. Samples MAR-24 and MAR-28C were not ploted.

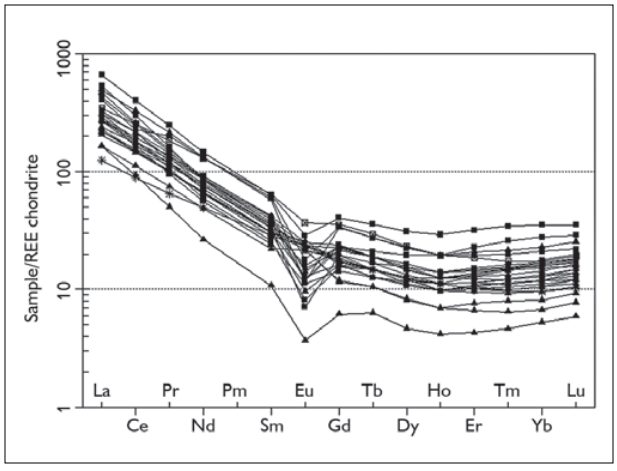

Figure 9. Rare earth elements plot by Boynton (1984) for syenites and phonolites of the Marapicu massif. Note general pattern with enrichment of light rare earth elements related to heavy rare earth elements and Eu negative anomaly. Triangle represents plutonic nepheline syenites and syenites, filled squares represents phonolites, open square and asterisk represents basic rocks.

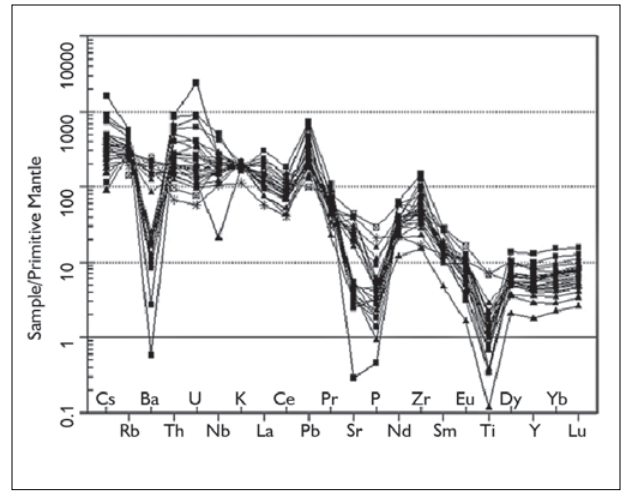

Figure 10. Spidergram primitive mantle normalized by Sun & McDonough (1989). Note depletion in Ba, Sr, P and Ti and enrichment of Rb, Th, U, Nb and Pb. Triangle represents plutonic nepheline syenites and syenites, filled squares represents phonolites, open square and asterisk represents basic rocks.

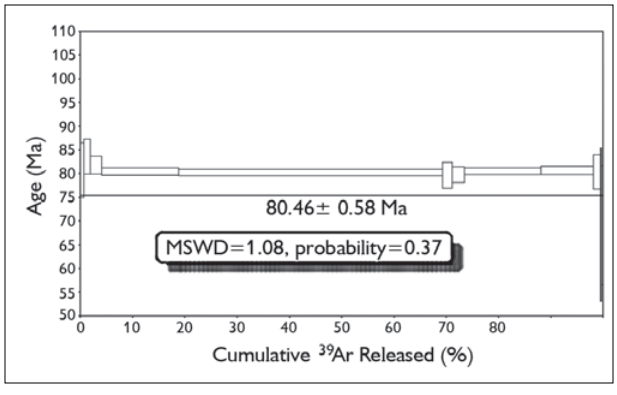

Figure 11. Age spectra showing plateau age of 80.46 ± 0.58 with a MSWD = 1.08.

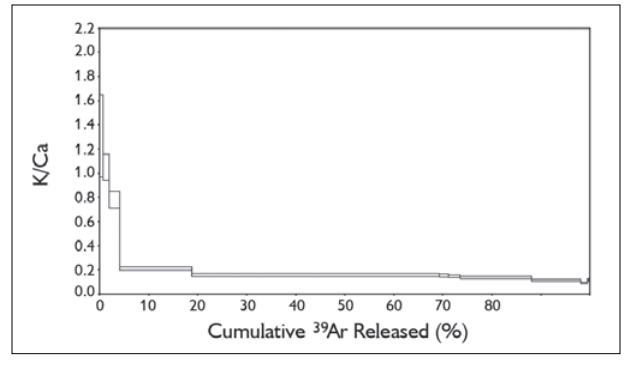

Figure 12. K/Ca ratio showing a K-rich component at the low-temperature steps and relatively constant compositions for the medium to high temperature steps.

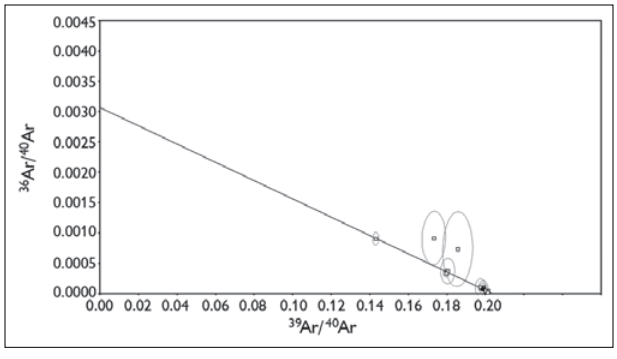

Figure 13. Inverse isochron with step heating data of hornblende providing the age of (80.27 ± 0.62 Ma).

Both Al_2O_3 and Na_2O presents higher concentrations in the most evaluated members (nepheline syenites and phonolites) whereas MgO, CaO, TiO_2 and P_2O_5 shows higher concentrations in syenites. Fe_2O_3 contents have no significant concentration difference for analyzed lithotypes. The negative linear correlation of Na_2O is related to the fractionation of the feldspar as a main mineral phase. The major elements presents poor linear correlation with silica (except for Na_2O and K_2O) according to their R^2 values which not permit to make reliable insights.

The variation diagrams presented in the Figure 8 shows the negative linear correlation for Rb, Pb, Th, Y and U whereas Ba, Sr and Eu presents data dispersion. U, Th, Pb e Rb are markedly more concentrated in the nepheline syenites and phonolites than in syenites, Y have not so clear behavior. For Sr, Ba and Eu the concentrations are less easily detachable among the lithotypes. The negative linear correlation observed for Rb is related to fractionating of K-feldspar, main modal phase in these rocks, decreasing of Y is coherent with fractionation of apatite which is an accessory phase present in the mode.

Light Rare earth elements are more fractionated than heavy rare earth elements indicating a mantle source enriched in these elements such as Enriched Mantle 1 (EM1), Enriched Mantle 2 (EM2) or Ocean Island Basalts (OIB). The multielement spidergram presented shows depletion for Ba, Sr, P and Ti whereas Th, U, Pb and Zr are enriched. Depletion for Ba is coherent with the fractionation of K-feldspar (also indicated by the Sr depletion), biotite and hornblende. Depletion for P is corroborating by apatite fractionation and Ti for titanite fractionation, all of these phases are presents in the modal assemblage. Both MAR-28C and MAR-24 samples have not genetic relationship with the studied series despite of their high REE content related to the other samples.

Both Sr and Nd isotopic data from literature (Morbidelli *et al*., 1995; Mota, 2008, 2012) corroborate a magma origin from an astenospheric mantle. Such isotopic studies also indicating preferentially enriched mantle sources as EM1 or EM2 and the Pb isotopic results suggest an array among Mid-Ocean Ridge Basalt (MORB), OIB and EM2, indicating a mixture of two mantle components. The Pb isotopic data from the Tristan da Cunha Island presents similarities with the Pb isotopic signatures from alkaline intrusions and it is different of the signature observed in the Trindade and Açores ocean islands.

Structural geology and geophysics studies (magnetometry and gravimetry) Mota (2008) indicate that alkaline intrusions have little geometric relationship with the structural features from the basement, where the contacts forming rounded boundaries moreover isotropic texture observed on the samples. On the other hand, the alkaline intrusion presents regional distribution suggesting agreement alignment with the regional structural features from Neoproterozoic Ribeira Orogen and in addition have close relationship with the Cenozoic sediments. This correlation may be genetically interpreted where the extensional stresses which forming the basins also would be that responsible for alkaline magma intrusions.

CONCLUSION

The $^{40}Ar/^{39}Ar$ age presented in this work is the older for Poços de Caldas-Cabo Frio magmatic lineament. This fact do not support the idea of age decreasing from west to east in this magmatic province (Herz, 1977; Thomaz Filho & Rodrigues, 1999) based on K-Ar ages. According to this model, the passage of the South American Plate over a hot spot would generate a perfectly age decreasing among the emplaced bodies. Indeed, considering the experimental errors associated with K-Ar ages (3 Ma), support this model. However, new methodologies applied to the alkaline rocks may bring different interpretations and contribute to the knowledge for these magmatic manifestations. This way, more accurate $^{40}Ar/^{39}Ar$ dating shows that Marapicu Massif with 80 Ma is older than Poços de Caldas and Itatiaia (K-Ar ages of 74.6 Ma and 73.1 Ma respectively) which would be older considering their geographic location. This data shows how complex is the passage of the hot spot through the continental crust.

The data presented in this work together with those already published lead for two probably models: the first model take account the existence of a mantle plume originated into the asthenosphere from enriched sources (probably of deep subduction of continental crust slabs in previous events). The hot spot ways was recorded on the continental crust, even though being less marked than oceanic crust, due to their greater thickness. Generally, the trajectory of the hot spots are responsible

for kimberlitics and lamproitics body generation besides the alkaline complexes and carbonatite. It is in agreement with this model the petrologic, isotopic and geochemistry data, and the $^{40}Ar/^{39}Ar$ age.

On the other hand, both isotopic and geochemistry data from Trindade may not enable relate the alkaline rocks from continent with this island rocks. The secondly proposed model, in agreement with the recent $^{40}Ar/^{39}Ar$ data, suggest a crustal flexure. In this way, the sediments deposited into the continental shelf trigged a stress so that flexure the continental crust producing deep fractures allowing the entering of the mantellic magmas. Thus, future geochronology works of the alkaline rocks will provide fundamental information to the understanding questions about southeast Brazilian alkaline rocks genesis.

ACKNOWLEDGEMENT

The present research work has been performed under the financial support of Rio de Janeiro State University, Brazil. Part of the fieldwork instruments, office materials, and the resources of the informatics is supported by the FAPERJ (Fundação de Amparo à Pesquisa do Estado do Rio de Janeiro, Carlos Chagas Filho). The chemical analyses were performed by Activation Laboratories Ltd., Ontario, Canada. The 40Ar/39Ar analyses were performed at the Western Australian Argon Isotope Facility at Curtin University. The authors are grateful to the above-mentioned institutions.

REFERENCES

ALMEIDA, F. F. M., 1976. The system of continental rifts bordering the Santos basin, Brazil. **Anais da Academia Brasileira de Ciências** 48(supl.): 15-26.

ALMEIDA, F. F. M., 1983. Relações tectônicas das rochas alcalinas mesozóicas da região meridional da Plataforma Sul-Americana. **Revista Brasileira de Geociências** 13(3): 139-158.

ALMEIDA, F. F. M., 1986. Distribuição regional e relações tectônicas do magmatismo pós-paleozóico no Brasil. **Revista Brasileira de Geociências** 16(4): 325-349.

ALMEIDA, F. F. M., 1991. O alinhamento magmático de Cabo Frio. **Atas do Simpósio de Geologia do Sudeste** 2: 423-428.

ALMEIDA, F. F. M., C. D. R. CARNEIRO & A. M. P. MIZUSAKI, 1996. Correlação do magmatismo da margem continental brasileira com o das áreas emersas adjacentes. **Revista Brasileira de Geociências** 26(3): 125-138.

BOYNTON, W. V., 1984. Cosmochemistry of the rare-earth elements: meteorite studies. In: P. HENDERSON (Ed.): **Rare-earth elements geochemistry**: 63-114. Elsevier, Amsterdam.

COX, K. G., J. D. BELL & R. J. PANKHURST, 1979. **The interpretation of igneous rocks**: 1-450. George Allen and Unwin, London.

FAINSTEIN, R. & C. P. SUMMERHAYES, 1982. Structure and origin of marginal banks off eastern Brazil. **Marine Geology** 46(3-4): 199-215.

FREITAS, R. O., 1947. **Jazimentos de rochas alcalinas da ilha de São Sebastião**: 1-244. Faculdade de Filosofia Ciências e Letras (Boletim 85, Geologia 3), São Paulo.

GIBSON, S. A., R. N. THOMPSON, O. H. LEONARDOS, A. P. DICKIN & J. G. MITCHELL, 1995. The Late Cretaceous impact of the Trindade mantle plume: evidence from large-volume, mafic, potassic magmatism in SE Brazil. **Journal of Petrology** 36: 189-229.

GORINI, M. A. & G. M. BRYAN, 1976. The tectonic fabric of the equatorial Atlantic and adjoining continental margins: gulf of Guinea to northeastern Brazil. **Anais da Academia Brasileira de Ciências Rio de Janeiro** 48(supl.): 101-119.

HERZ, N., 1977. Timing of spreading in the South Atlantic: information from Brazilian alkalic rocks. **Geological Society of America Bulletin** 88(1): 101-112.

KLEIN, V. C., 1993. **O vulcão alcalino de Nova Iguaçu (estado do Rio de Janeiro)**: controle estrutural e processo de erupção. Tese (Doutorado em Geociências) – Universidade Federal do Rio de Janeiro, Rio de Janeiro.

KLEIN, V. C. & A. C. VIEIRA, 1980. Vulcões do Rio de Janeiro: breve geologia e perspectivas. **Mineração e Metalurgia** 419: 44-46.

KOPPERS, A. A. P., 2002. ArArCALC-software for $^{40}Ar/^{39}Ar$ age calculations. **Computers and Geosciences** 28(5): 605-619.

LEE, J. Y., K. MARTI, J. P. SEVERINGHAUS, K. KAWAMURA, H.-S. YOO, J. B. LEE, J. S. KIM, 2006. A redetermination of the isotopic abundance of atmospheric Ar. **Geochimica et Cosmochimica Acta** 70(17): 4507-4512.

MORBIDELLI, L., C. B. GOMES, L. BECCALUVA, P. BROTZU, A. M. CONTE, E. RUBERTI & G. TRAVERSA, 1995. Mineralogical, petrological and geochemical aspects of alkaline and alkaline-carbonatite associations from Brazil. **Earth-Science Reviews** 39(3-4): 135-168.

MOTA, C. E. M., 2008. **Estudos geológicos e gravimétricos do Complexo Marapicu-Gericinó-Mendanha, Rio de Janeiro**. Dissertação (Mestrado em Análise de Bacias e Faixas Móveis) – Universidade do Estado do Rio de Janeiro, Rio de Janeiro.

MOTA, C. E. M., 2012. **Petrogênese e geocronologia das intrusões alcalinas de Morro Redondo, Mendanha e Morro de São João**: caracterização do magmatismo alcalino no estado do Rio de Janeiro e implicações geodinâmicas. Tese (Doutorado em Geologia) – Universidade do Estado do Rio de Janeiro, Rio de Janeiro.

RENNE, P. R., R. MUNDIL, G. BALCO, K. MIN & K. R. LUDWIG, 2010. Joint determination of ^{40}K decay constants and $^{40}Ar^*/^{40}K$ for the Fish Canyon sanidine standard, and improved accuracy for $^{40}Ar/^{39}Ar$ geochronology. **Geochimica et Cosmochimica Acta** 74(18): 5349-5367.

SHAND, S. J., 1943. **Eruptive rocks**. Their genesis, composition, classification, and their relation to ore-deposits with a chapter on meteorite. John Wiley and Sons, New York.

SUN, S. S. & W. F. MCDONOUGH, 1989. Chemical and isotopic systematics of oceanic basalts: implications for mantle composition and processes. **Geological Society** 42: 313-345.

THOMAZ FILHO, A. & A. L. RODRIGUES, 1999. O alinhamento de rochas alcalinas Poços de Caldas-Cabo Frio (RJ) e sua continuidade na cadeia Vitória Trindade. **Revista Brasileira de Geociências** 29(2): 275-280.

THOMAZ FILHO, A., A. M. P. MIZUSAKI, E. J. MILANI & P. CESERO, 2000. Rifting and magmatism associated with the South America and Africa breakup. **Revista Brasileira de Geociências** 30(1): 17-19.

THOMAZ FILHO, A., E. GUEDES, M. HEILBRON, P. M. VASCONCELOS, C. M. VALERIANO, J. C. H. ALMEIDA & W. TEIXEIRA, 2005. K–Ar and $^{40}Ar/^{39}Ar$ ages of dikes emplaced in the onshore basement of the Santos Basin, Resende area, SE Brazil: implications for the south Atlantic opening and Tertiary reactivation. **Journal of South American Earth Sciences** 18(3-4): 371-382.

THOMPSON, R. N., S. A. GIBSON, J. G. MITCHELL, A. P. DICKIN, O. H. LEONARDOS, J. A. BROD & J. C. GREENWOOD, 1998. Migrating Cretaceous-Eocene magmatism in the Serra do Mar Alkaline Province, SE Brazil: melts from the deflected Trinidade mantle plume? **Journal of Petrology** 39: 1493-1526.

ULBRICH, H. H. G. J. & C. B. GOMES, 1981. Alkaline rocks from continental Brazil. **Earth-Science Reviews** 17(1-2): 135-154.

APPENDIX. Geochemistry data of the 27 analyzed samples from Marapicu massif, classification is according to Cox *et al*. (1979). (Continue)

Analyte symbol	Classification	(Na+K)/Al mol	SiO_2	Al_2O_3	Fe_2O_3 (T)	MnO	MgO	CaO	Na_2O	K_2O	TiO_2	P_2O_5	LOI	Total	Sc	Pb	V
MAR-28C	Basanite/ tephrite	0.75179718	47.5	15.55	8.24	0.157	7.02	8.51	4.87	3.39	1.541	0.45	2.01	99.24	20	13	183
MAR-01D	Nepheline syenite	0.94861556	59.94	20.17	3.96	0.161	0.05	1.2	7.62	6.08	0.073	0.02	1.11	100.4	< 1	17	< 5
MAR-03	Nepheline syenite	0.90494555	59.07	18.51	5.64	0.206	0.27	1.77	6	6.34	0.229	0.1	1.41	99.54	< 1	14	< 5
MAR-10B	Nepheline syenite	0.9372604	57.43	21.72	2.91	0.127	0.06	0.92	8.72	5.54	0.081	0.04	1.23	98.79	< 1	19	< 5
MAR-17B	Nepheline syenite	0.95989968	58.94	19.03	5.11	0.204	0.08	1.31	7.39	5.63	0.145	0.05	0.69	98.56	< 1	9	< 5
MAR-19A	Nepheline syenite	0.94660567	61.36	20.59	1.92	0.051	0.04	0.41	8.18	5.56	0.025	0.05	0.48	98.68	< 1	16	< 5
MAR-27	Nepheline syenite	0.86729414	57.17	17.79	7.07	0.223	0.89	2.49	5.83	5.38	0.618	0.34	2.17	99.97	2	17	19
MAR-02B	Phonolite	1.11998785	54.09	20.09	3.85	0.233	0.08	0.92	9.66	6.09	0.244	0.03	3.95	99.22	< 1	42	< 5
MAR-04C	Phonolite	0.99073902	56.63	19.24	4.88	0.204	0.18	1.35	7.55	6.12	0.176	0.07	2.84	99.26	< 1	20	< 5
MAR-05A	Phonolite	0.96885795	56.4	19.28	4.94	0.209	0.17	1.32	7.41	5.98	0.171	0.07	2.5	98.44	< 1	21	< 5
MAR-06A	Phonolite	0.90939645	57.35	19.2	4.14	0.149	0.35	1.87	6.57	6.13	0.418	0.11	2.09	98.38	< 1	17	< 5
MAR-07	Phonolite	0.91783444	57.75	19.84	4.3	0.155	0.36	1.85	6.92	6.29	0.447	0.13	2.1	100.1	< 1	16	6
MAR-09A	Phonolite	1.05440313	57.23	20.35	3.66	0.175	0.12	0.98	9.25	5.75	0.148	0.04	1.57	99.28	< 1	31	< 5
MAR-15	Phonolite	1.18632374	53.46	19.38	4.74	0.285	0.08	1.08	10.71	4.95	0.246	0.04	4.01	98.99	< 1	52	< 5
MAR-18	Phonolite	1.0163233	56.06	20.88	3.75	0.198	0.02	1.05	9.08	5.79	0.073	0.01	1.28	98.2	< 1	26	< 5
MAR-19B	Phonolite	0.95590523	57.15	19.1	4.13	0.169	0.17	1.43	7.18	5.94	0.258	0.06	3.16	98.76	< 1	23	< 5
MAR-22B	Phonolite	0.93557036	58.72	18.49	5.73	0.238	0.45	1.94	6.63	5.89	0.475	0.2	0.92	99.68	< 1	13	< 5
MAR-22C	Phonolite	1.03139422	56.41	20.3	3.27	0.134	0.15	1.04	9	5.65	0.263	0.07	2.61	98.9	< 1	34	5
MAR-28B	Phonolite	1.0424381	57.44	19.5	4.45	0.19	0.27	1.24	8.88	5.27	0.382	0.09	1.56	99.27	1	49	10
MAR-24	Phonolitic tephrite	0.82921419	52.35	16.78	9.01	0.274	2.5	5.66	5.14	5.03	1.493	0.63	1.08	99.95	8	7	121
MAR-01A	Syenite	0.91943998	61.02	18.38	3.72	0.128	0.23	1.64	6.13	6.28	0.255	0.09	1.08	98.95	< 1	13	< 5
MAR-06B	Syenite	0.90082148	61.18	19.3	3.03	0.096	0.17	1.33	6.34	6.41	0.209	0.09	0.95	99.1	< 1	10	< 5
MAR-13C	Syenite	0.92133899	60.06	18.7	4.16	0.141	0.29	1.69	6.37	6.22	0.302	0.11	0.86	98.9	< 1	13	< 5

APPENDIX. (Continue)

Analyte symbol	Classification	(Na+K)/Al mol	SiO_2	Al_2O_3	Fe_2O_3 (T)	MnO	MgO	CaO	Na_2O	K_2O	TiO_2	P_2O_5	LOI	Total	Sc	Pb	V
MAR-16A	Syenite	0.91976099	61.87	19.29	3.34	0.109	0.2	1.46	6.55	6.42	0.214	0.08	0.69	100.2	< 1	14	< 5
MAR-16C	Syenite	0.90107464	60.8	18.25	4.67	0.155	0.36	1.85	5.88	6.24	0.318	0.1	0.72	99.35	< 1	15	< 5
MAR-20	Syenite	0.89372099	59.26	18.22	4.83	0.171	0.27	1.83	5.98	5.94	0.28	0.13	1.6	98.51	< 1	15	< 5
MAR-26	Syenite	0.89495522	58.49	18.11	4.72	0.148	0.63	2.17	6.29	5.4	0.465	0.24	2.35	99.01	2	15	19

Analyte symbol	Classification	Ba	Sr	Y	Zr	Cr	Co	Ni	Cu	Zn	Ga	Ge	As	Rb	Nb	Mo	Th	In	Sn
MAR-28C	Basanite/ tephrite	1316	833	20	188	370	37	130	70	90	18	1	< 5	120	75	2	5.7	< 0.2	2
MAR-01D	Nepheline syenite	83	83	21	517	< 20	35	< 20	< 10	120	28	1	< 5	166	115	< 2	20.8	< 0.2	7
MAR-03	Nepheline syenite	124	92	26	551	< 20	37	< 20	< 10	110	23	2	< 5	175	169	3	17	< 0.2	4
MAR-10B	Nepheline syenite	174	112	27	498	< 20	23	< 20	< 10	100	30	2	< 5	206	110	3	35.2	< 0.2	5
MAR-17B	Nepheline syenite	118	79	39	877	< 20	77	< 20	< 10	130	31	2	< 5	176	203	< 2	42.7	< 0.2	8
MAR-19A	Nepheline syenite	62	62	8	166	< 20	28	< 20	< 10	40	29	1	< 5	215	15	< 2	16.3	< 0.2	2
MAR-27	Nepheline syenite	1006	605	26	553	< 20	19	< 20	< 10	150	23	2	< 5	178	154	3	16.2	< 0.2	4
MAR-02B	Phonolite	19	74	44	1399	< 20	25	< 20	< 10	180	42	2	8	332	302	13	49.2	< 0.2	11
MAR-04C	Phonolite	59	59	29	583	< 20	19	< 20	< 10	120	26	2	< 5	199	156	5	20.3	< 0.2	4
MAR-05A	Phonolite	117	52	36	606	< 20	37	< 20	< 10	130	28	2	< 5	208	170	7	22.6	< 0.2	5
MAR-06A	Phonolite	1531	838	20	517	< 20	30	< 20	< 10	100	22	1	< 5	173	104	3	15.3	< 0.2	3
MAR-07	Phonolite	1539	837	22	546	< 20	40	< 20	< 10	110	24	1	< 5	185	114	3	16.3	< 0.2	3
MAR-09A	Phonolite	76	62	25	779	< 20	22	< 20	< 10	130	30	2	< 5	258	151	3	34.1	< 0.2	6
MAR-15	Phonolite	67	82	59	1658	< 20	48	< 20	< 10	240	43	2	11	365	353	21	71.8	< 0.2	11
MAR-18	Phonolite	4	6	30	616	< 20	26	< 20	< 10	130	30	1	< 5	238	136	2	23.5	< 0.2	6
MAR-19B	Phonolite	133	115	22	737	< 20	102	< 20	< 10	120	26	1	< 5	216	123	10	23.7	< 0.2	5
MAR-22B	Phonolite	1350	393	28	458	< 20	13	< 20	< 10	160	27	2	< 5	193	140	< 2	17.3	< 0.2	6

APPENDIX. (Continue)

Analyte symbol	Classification	Ba	Sr	Y	Zr	Cr	Co	Ni	Cu	Zn	Ga	Ge	As	Rb	Nb	Mo	Th	In	Sn
MAR-22C	Phonolite	142	106	24	1018	< 20	24	< 20	< 10	120	32	1	< 5	283	191	5	53.1	< 0.2	5
MAR-28B	Phonolite	123	100	27	1140	< 20	39	< 20	< 10	200	39	2	< 5	344	183	< 2	76.2	< 0.2	10
MAR-24	Phonolitic tephrite	1693	920	36	431	< 20	23	30	20	150	23	2	< 5	90	145	3	8.2	< 0.2	3
MAR-01A	Syenite	1066	511	19	383	< 20	23	< 20	< 10	70	21	1	< 5	155	105	2	13.1	< 0.2	3
MAR-06B	Syenite	1124	533	13	249	< 20	29	< 20	< 10	50	20	1	< 5	141	76	3	10.4	< 0.2	2
MAR-13C	Syenite	1048	472	18	308	< 20	59	< 20	< 10	70	21	1	< 5	152	106	3	13.5	< 0.2	3
MAR-16A	Syenite	1283	617	16	371	< 20	14	< 20	< 10	60	19	1	< 5	140	86	6	12	< 0.2	2
MAR-16C	Syenite	586	338	20	354	< 20	17	< 20	< 10	80	21	1	< 5	167	121	< 2	12.2	< 0.2	3
MAR-20	Syenite	1035	446	21	409	< 20	46	< 20	< 10	90	23	2	< 5	200	118	4	13.6	< 0.2	4
MAR-26	Syenite	867	546	22	566	< 20	23	< 20	< 10	90	22	1	< 5	160	120	4	22.8	< 0.2	3

Analyte symbol	Classification	Sb	Cs	La	Ce	Pr	Nd	Sm	Eu	Gd	Tb	Dy	Ho	Er	Tm	Yb	Lu	Hf	U
MAR-28C	Basanite/ tephrite	< 0.5	2.9	38.9	72.1	7.97	29.7	5.6	1.74	4.8	0.7	4	0.8	2.1	0.31	2	0.33	4.3	1.2
MAR-01D	Nepheline syenite	0.6	1.2	96.4	175	14.7	42.9	5.9	0.71	4.2	0.6	3.6	0.7	2.2	0.37	2.5	0.39	11.6	4.2
MAR-03	Nepheline syenite	< 0.5	2.2	85.3	159	16.7	54.3	8.2	1.04	6	0.9	5	0.9	2.7	0.43	3	0.53	12.1	3
MAR-10B	Nepheline syenite	< 0.5	3.3	146	211	18.8	52.6	7.2	1.1	5.6	0.9	5	1	3	0.47	3.2	0.51	10.9	6.8
MAR-17B	Nepheline syenite	< 0.5	0.7	154	267	26.1	79.4	11.3	0.85	8.7	1.3	7.4	1.4	4.4	0.7	4.8	0.82	17.7	8.2
MAR-19A	Nepheline syenite	< 0.5	2.7	51.4	75.7	6.13	15.9	2.1	0.27	1.6	0.3	1.5	0.3	0.9	0.15	1.1	0.19	3.5	2.4
MAR-27	Nepheline syenite	< 0.5	3.6	85.3	143	15.8	51.8	7.7	1.7	5.9	0.9	4.7	0.9	2.6	0.39	2.7	0.48	11.4	4
MAR-02B	Phonolite	0.6	7.1	165	243	19.8	50.7	6.5	1.18	6	1	6.3	1.4	4.8	0.84	5.8	0.93	25.7	13
MAR-04C	Phonolite	< 0.5	3	89.3	159	16.4	52.7	8	0.89	6.1	0.9	5.3	1	3.1	0.49	3.3	0.56	11.7	4.9
MAR-05A	Phonolite	< 0.5	3.8	127	184	24.5	78.5	11.7	1.32	8.9	1.3	7.2	1.4	4.1	0.64	4.4	0.71	13	5.4

APPENDIX. (Conclusion)

Analyte symbol	Classification	Sb	Cs	La	Ce	Pr	Nd	Sm	Eu	Gd	Tb	Dy	Ho	Er	Tm	Yb	Lu	Hf	U
MAR-06A	Phonolite	< 0.5	2	68.8	122	12.4	39.3	5.5	1.77	4.3	0.6	3.5	0.7	2.1	0.34	2.3	0.39	10.1	3.5
MAR-07	Phonolite	< 0.5	2.4	83.6	136	14.4	45.6	6.4	1.82	4.5	0.7	3.9	0.7	2.3	0.37	2.5	0.42	10.6	3.7
MAR-09A	Phonolite	< 0.5	3.9	95.7	149	13	35.8	5	0.6	4	0.7	4	0.9	2.8	0.49	3.5	0.59	14.8	8.6
MAR-15	Phonolite	0.8	12.7	206	326	30.1	87.4	12.3	2.1	10.5	1.7	10	2.1	6.7	1.12	7.4	1.14	29.5	18.9
MAR-18	Phonolite	< 0.5	2.7	103	173	15.9	46.4	6.4	0.52	5.1	0.8	5	1	3.2	0.53	3.5	0.58	12.4	5.5
MAR-19B	Phonolite	< 0.5	3.9	86.2	149	14.3	43	6	0.95	4.2	0.7	3.9	0.8	2.4	0.4	2.8	0.48	14.4	5.3
MAR-22B	Phonolite	< 0.5	0.9	101	175	17.4	55	8.1	1.83	6.2	0.9	5.3	1	3.1	0.5	3.3	0.55	11.6	3.4
MAR-22C	Phonolite	< 0.5	5.9	89.8	136	11.7	33.6	4.7	0.83	3.7	0.6	3.8	0.8	2.7	0.47	3.4	0.57	18	17.5
MAR-28B	Phonolite	0.5	6	133	206	18	50.6	7.2	0.88	5.7	0.9	4.8	0.9	2.9	0.49	3.7	0.64	21.3	50
MAR-24	Phonolitic tephrite	< 0.5	< 0.5	108	206	22.5	77.9	12.5	2.71	9.2	1.4	7.5	1.4	3.9	0.56	3.6	0.62	10.4	1.6
MAR-01A	Syenite	< 0.5	2.1	71	125	12.2	39.6	5.9	1.89	4.5	0.7	3.6	0.7	2.1	0.32	2.2	0.36	8.4	3
MAR-06B	Syenite	< 0.5	1.4	51.4	91.1	9.09	29.2	4.3	1.59	3	0.5	2.6	0.5	1.4	0.21	1.4	0.25	5.5	2
MAR-13C	Syenite	< 0.5	1.8	63.8	118	12.3	40.2	6	1.74	4.4	0.7	3.6	0.7	2	0.3	2	0.34	7.2	2.7
MAR-16A	Syenite	< 0.5	1.6	51.1	90.5	9.09	29.3	4.3	1.61	3.1	0.5	2.7	0.5	1.6	0.26	1.7	0.3	6.8	2.2
MAR-16C	Syenite	< 0.5	1.8	67.3	127	13.6	45.5	6.9	1.68	5.1	0.7	4.1	0.7	2.2	0.32	2.2	0.39	8.2	2.2
MAR-20	Syenite	< 0.5	2.5	74.2	141	14.6	47.6	7	1.55	5.1	0.8	4.3	0.8	2.4	0.36	2.5	0.45	9.3	2.7
MAR-26	Syenite	< 0.5	2.4	68.3	120	12	38.9	6	1.6	4.6	0.7	3.9	0.8	2.4	0.39	2.7	0.45	10.1	7.4